DOI: 10.1002/((please add manuscript number))
Article type: Communication

Dielectric Polarization in Inverse Spinel-Structured Mg_2TiO_4 Coating to Suppress Oxygen Evolution of Li-Rich Cathode Materials

Wei Zhang, Yonggang Sun, Huiqiu Deng, Jianming Ma, Yi Zeng, Zhiqiang Zhu, Zhisheng Lv, Huarong Xia, Xiang Ge, Shengkai Cao, Yao Xiao, Shibo Xi, Yonghua Du, Anmin Cao and Xiaodong Chen**

[*] Dr. W. Zhang, Dr. Y. Zeng, Dr. Z. Zhu, Dr. Z. Lv, Dr. H. Xia, Dr. X. Ge, Dr. S. Cao, Dr. Y. Xiao, Prof. X. Chen
Innovative Centre for Flexible Devices, School of Materials Science and Engineering, Nanyang Technological University, 50 Nanyang Avenue, Singapore 639798, Singapore
E-mail: chenxd@ntu.edu.sg
Webpage: http://www.ntu.edu.sg/home/chenxd/

Dr. Y. Sun, Prof. A. Cao
CAS Key Laboratory of Molecular Nanostructure and Nanotechnology, and CAS Research/Education Center for Excellence in Molecular Sciences, Institute of Chemistry, Chinese Academy of Sciences (CAS), and Beijing National Laboratory for Molecular Sciences (BNLMS), Beijing 100190, China
E-mail: anmin_cao@iccas.ac.cn

Prof. H. Deng, Prof. J. Ma
School of Physics and Electronics, Hunan University, Changsha 410082, China

Dr. S. Xi
Institute of Chemical and Engineering Sciences Institution 1 Pesek Road, Jurong Island, Singapore 627833, Singapore

Dr. Y. Du
National Synchrotron Light Source II, Brookhaven National Laboratory Upton NY, 11973 USA

Keywords: dielectric polarization, cathode materials, oxygen release, surface modification, lithium-ion batteries

Abstract

High-energy Li-rich layered cathode materials (~900 Wh/kg) suffer from severe capacity and voltage decay during cycling, which is associated with layered-to-spinel phase transition and oxygen redox reaction. Current efforts mainly focus on surface modification to suppress this unwanted structural transformation. However, the true challenge probably originates from the

continuous oxygen release upon charging. Here we report using dielectric polarization in surface coating to suppress the oxygen evolution of Li-rich material, using Mg_2TiO_4 as a proof-of-concept material. The creation of a reverse electric field in surface layers effectively restrain the outward migration of bulk oxygen anions. Meanwhile, high oxygen-affinity elements of Mg and Ti well stabilize the surface oxygen of Li-rich material via enhancing the energy barrier for oxygen release reaction, verified by density functional theory simulation. Benefited from these, the modified Li-rich electrode exhibits an impressive cyclability with a high capacity retention of ~81% even after 700 cycles at 2 C (~0.5 A/g), far superior to ~44% of the unmodified counterpart. In addition, Mg_2TiO_4 coating greatly mitigates the voltage decay of Li-rich material with the degradation rate reduced by ~65%. This work proposes new insights into manipulating surface chemistry of electrode materials to control oxygen activity for high-energy-density rechargeable batteries.

Li-rich layered oxides ($xLi_2MnO_3 \cdot (1-x)LiMO_2$, M= Mn, Ni, Co) are among the leading cathode candidates for high energy lithium-ion batteries (LIBs) due to the high specific capacities of ~280 mAh/g, nearly double that of conventional cathode materials $LiCoO_2$ and $LiMn_2O_4$.[1] The extra capacity originates from the redox reactions of anionic oxygen (O^{2-}/O_2^{n-}, where $1< n <3$), besides the cationic contribution.[2] However, one major bottleneck is severe capacity and voltage fading during cycling, which is due to the side reaction between electrode/electrolyte, layer-to-spinel phase transition, and oxygen evolution.[3] Current efforts mainly focus on solving the first two problems. Various surface protection layers were developed to mechanically restrict this unwanted structural degradation and prevent the cathode from the hydrofluoric acid attack of electrolyte, including oxides (e.g., Al_2O_3, MgO, TiO_2), phosphates ($AlPO_4$, $FePO_4$, $LiFePO_4$) and fluorides (AlF_3, LiF, MgF_2).[4] Unfortunately, the root cause of the issue probably originates from the third one, oxygen release during the

charging process.[5] Therefore, suppressing this continuous oxygen loss remains a significant challenge.

To tackle this, we delved into the whole process of oxygen evolution upon charging in detail. It consists of two main steps. The first step is surface oxygen evolution. Under-coordinated oxygen at the surface is prone to decompose into oxygen gas via breaking Li-O and transition metal-oxygen (M-O) bonds and forming new O-O bonds (**Scheme 1**a).[6] The spontaneity of the chemical reaction is determined by the change in Gibbs free energy of the process (ΔG) in thermodynamics Eq. (1),[7]

$$\Delta G = \Delta H - T\Delta S = xBE_{Li-O} + yBE_{M-O} - \frac{x+y}{2}BE_{O-O} - T\Delta S \quad (1)$$

where ΔH represents the change in enthalpy, ΔS means the change in entropy, T is the temperature in Kelvin, and BE_A denotes the bond energy (A= Li-O, M-O, and O-O). The higher the value of ΔG, the more thermodynamically unfavorable the reaction is. Surface modification with high oxygen-affinity elements to increase bond energies of the reactants is an attractive strategy to make the oxygen evolution energetically unfavorable (Scheme 1b).[8] The second step is bulk oxygen anions migrated toward the surface and caused subsequent oxygen release.[5g, 9] Under the external electrical field, oxygen anions in the subsurface layers gradually migrate to the outmost surface mediated by oxygen vacancies, and this progressively expands inward to the bulk region during prolonged cycling, resulting in continuous oxygen loss.[10] Considering the external electric field is the driving force for the outward migration of bulk oxygen, the key to suppressing the continuous oxygen loss lies in reducing the effect of the electric field on the electrode surface. This can be realized by the dielectric polarization of coating, in which electrical dipoles in the coating materials tend to align themselves to form a reverse electric field (Scheme 1c).[11] To form a heterostructure, lattice match between core and shell is an essential requirement.[12] In terms of anion arrangement, spinel oxide exhibits the same cubic close-packed oxygen structure with layered Li-rich materials, which is a promising

candidate for coating (Scheme 1d).[13] For cations selection corresponding to both lithium and transition-metal sites, it needs to satisfy the following two criteria. Metal ions in the shell should be of nearly the same size as that in Li-rich material and they should exhibit a higher affinity to oxygen (Scheme 1e,f).[14]

Herein, we demonstrated that dielectric inverse spinel structured Mg_2TiO_4 coating, in which a reverse electrical field is formed to restrict the outward migration of bulk anions, effectively suppressed the continuous oxygen release of Li-rich materials. High oxygen-affinity elements Mg and Ti well stabilized surface oxygen of Li-rich cathode materials via enhancing the energy barrier of oxygen evolution reaction, according to density functional theory (DFT) simulation. Impressively, this modified Li-rich electrode exhibited unprecedented cyclability with a capacity retention of ~81% after 700 cycles at 2 C (1 C= 250 mA/g), far superior to ~44% of the unmodified counterpart. Meanwhile, the Mg_2TiO_4-coated Li-rich electrode displayed significantly mitigated voltage decay with the degradation of only 0.21 mV per cycle at 2 C, compared to 0.62 mV per cycle of the bare electrode. This work heralds a new paradigm of stabilizing anions via interface chemistry manipulation for high-energy-density electrode materials towards practical applications.

In a typical experiment, commercial Li-rich material $Li_{1.2}Mn_{0.54}Ni_{0.13}Co_{0.13}O_2$ (LR) was used as core materials, and Mg_2TiO_4 (MTO) surface coating was realized via a coprecipitation method according to the literature.[15] After thermal treatment at 550 ^oC, the final product Mg_2TiO_4-coated Li-rich material (LR@MTO) was obtained (Figure S1). The spherical morphology remained almost unchanged after modification according to scanning electron microscopy (SEM) (Figure S2). But the surface of LR@MTO particles became smoother and a thin layer of low-conductivity materials could be discerned. The chemical compositions of the coating were analyzed by energy dispersive spectroscopy (EDS) elemental mapping, which composed of Mg, Ti, and O (**Figure 1**a). These could be further verified by X-ray photoelectron spectroscopy (XPS) (Figure S3) and elemental mapping in scanning transmission electron

microscopy (STEM) mode (Figure S4). Meanwhile, the spinel MTO coating displayed a good lattice match with layered LR material (Figure 1b, S5, S6), which could potentially provide throughout protection. To eliminate the possible elemental doping during the coating process, we further investigated the bulk structure via X-ray absorption spectroscopy (XAS). Both samples exhibited nearly identical features of X-ray absorption near edge structure (XANES) and extended X-ray absorption fine structure spectra (EXAFS) (Figure 1c,d, S7), suggesting that no ions of MTO penetrated into the lattice of LR during the coating process. This could be further demonstrated by X-ray diffraction (XRD) results and the corresponding Rietveld refinements (Figure 1e, Table S1). Both patterns revealed the characteristic diffraction reflections of a well-crystallized layered structure with $R\bar{3}m$ symmetry. All these results demonstrated the successful introduction of MTO on the surface of LR material, with bulk structure well maintained.

To evaluate the impact of MTO coating on the oxygen evolution in LR, we first studied the thermal stability of both LR and LR@MTO electrodes at the charged state, since the thermal decomposition of cathode materials was closely related to oxygen release.[16] In-situ XRD was carried out to monitor the structure change of LR and LR@MTO electrode materials during the heating experiment every 20 ^{o}C from 40 to 600 ^{o}C (Figure S8). Special attention was paid to the typical (003) reflection, which is indexed with the regular layered structure of LR material. Initially, the reflection of both samples shifted to smaller angles (**Figure 2**a, 2b), because the repulsive interaction between oxygen atomic layers became much stronger with the increased temperature. When the temperature reached a critical value, the reflection suddenly started to shift towards larger angles, indicative of the emergence of a new reflection corresponding to (111) phase plane of the spinel structure. This inflection point could serve as an indicator of the layered-to-spinel phase transition due to the oxygen release, which was elevated by ~100 ^{o}C for LR@MTO compared to uncoated LR. Differential scanning calorimetry (DSC) was also used to study the thermal stability of both fully-charged electrodes. The temperature of exothermic

peak related to oxygen evolution is greatly increased after MTO coating, and the heat release is largely reduced by ~35%, from 342 down to 253 J/g (Figure 2c, 2d). Since oxygen evolution during the charging process would cause the microstructure transformation of Li-rich material, in situ XRD was further performed to directly monitor the phase change of both bare and modified LR electrodes at the first delithiation/lithiation cycle (Figure 2e, 2f). Upon charging, the (003) reflection initially shifted to lower scattering angles, indicating an expansion of c-lattice due to the intensified electrostatic repulsive force between oxygen anions after the removal of lithium. Then the reflection started to shift toward high angles as the voltage increased, corresponding to the lattice contraction because of oxygen release, which is significantly inhibited after MTO surface coating. All these proved that the oxygen release of Li-rich material was greatly alleviated after MTO coating.

Considering oxygen loss would reduce the oxidation states of cations according to the principles of charge neutrality, the valence of transition metals can serve as another indicator for oxygen release, especially Mn. XPS was first carried out to detect the valance state of Mn in both as-prepared and post-cycled electrodes (**Figure 3**a, 3b). After XPS deconvolution, quantitative information of the Mn^{3+}/Mn^{4+} ratio can be obtained. For the freshly prepared electrodes, Mn^{3+} only accounts for ~20% of the total manganese for both samples. But after charging/discharging at 2 C (~0.5 A/g) for 200 cycles, the ratio of Mn^{3+} for bare LR electrode was significantly increased to nearly 50% of total manganese, compared with ~25% of LR@MTO (Figure 3c). This was further confirmed by XAS, the pre-edge features of which could also provide the valence information and coordination environment (Figure 3d). The edge position of LR@MTO shifts to higher photon energy and the smaller increment of pre-edge intensity compared to LR , indicating a higher Mn valence state and alleviated oxygen loss for the modified sample (Figure 3e). In addition, the morphology change with cycling was monitored by TEM. Initially, both LR and LR@MTO exhibited similar morphology (Figure S9). But after 200 cycles, the LR electrode particles became very porous (Figure 3f), while

LR@MTO still maintained very decent morphology (Figure 3g), directly revealing the suppressed oxygen release after coating. Electron energy loss spectroscopy (EELS) analysis was further utilized to detect the oxidation state of Mn point-by-point in LR (Figure 3h). The position of Mn EELS peak at the pore edge shift to smaller photon energy compared to that in bulk materials (Figure 3i), indicative of lower valence state of Mn. This demonstrated that the porous structure after cycling is because of oxygen release. All the above results proved that the oxygen loss of LR is significantly alleviated after MTO modification.

To correlate the suppressed oxygen evolution with MTO surface coating, we carried out density functional theory (DFT) calculations to study the oxygen loss on the surface of bare and modified LR. The stoichiometric clean and MTO-covered LR (003) surfaces were used, with a vacuum layer to avoid virtual interaction. And the relaxed crystal structures were depicted in **Figure 4**a, 4b. Three different types of oxygen positions were chosen, including sites bonding to Ti, adjacent to Mg atom, and detached to both Mg and Ti. The formation energy (ΔE_o) of oxygen vacancy (Vo) was calculated by the following equation [Eq. (3)]:

$$\Delta E_o = E_{Vo} + \frac{1}{2}E_{O_2} - E_0 \qquad (2)$$

where E_{Vo} is the total energy of (003) surface with one oxygen vacancy per supercell, E_{O_2} is the energy of the gas phase O_2 molecule, E_0 is the energy of the supercell without oxygen vacancy. The formation energies of oxygen vacancy at these three sites were significantly increased by 0.31, 0.08, and 1.12 eV, respectively (Figure 4c), suggesting that the oxygen loss in Li-rich cathode became energetically unfavorable after MTO coating (Figure 4d).

Considering whatever the voltage decay or capacity loss is closely connected with the oxygen release, electrochemical performance of LR and LR@MTO electrodes could serve as another evidence to evaluate the oxygen release. CR2032 coin cells were assembled using lithium metal as anode and LR or LR@MTO as cathode. The similar cyclic voltammograms of

both electrodes at a sweep rate of 0.1 $mV \cdot s^{-1}$ within the potential range from 2 to 4.9 V, demonstrated that surface modification didn't change the bulk structure of Li-rich material (**Figure 5**a). When varying the amount of MTO coating from 0, 0.2wt%, 0.5wt%, 1wt% to 5wt%, the charging capacities in the first cycle at a current density of 0.1 C (1 C = 250 mA/g) were 334, 325, 323, 319 and 303 mAh/g, respectively (Figure 5b). This indicated that the initial oxygen release from the Li-rich lattice framework was to some extent alleviated after MTO coating, which became more pronounced with the increased amount of coating. In the meantime, thick MTO layers on the Li-rich material would sacrifice the rate performance (Figure S10, S11). For instance, LR@MTO5 (5wt%) electrode could only deliver a discharging capacity of 132 mAh/g at 5 C, far interior to 185 mAh/g of the bare counterpart (Figure 5c). Therefore, the coating amount of MTO should be controlled within an appropriate range and 1wt% was chosen in further experiments. It is generally acknowledged that LR cathode suffers from severe voltage decay upon cycling, which is a key obstacle for its commercialization. So we detailed compared the charging-discharging curves for LR and LR-MTO at 2 C (~0.5 A/g) for the 2^{nd}, 40^{th}, 80^{th}, 120^{th}, $160^{th,}$ and 200^{th} cycles (Figure 5d, 5e) and calculated the average working voltages verse the cycle number (Figure 5f). The discharging voltage deteriorated approximately 432 mV between the 1st and the 700^{th} cycles for bare LR, whereas the voltage decayed only 151 mV for LR@MTO, indicting the mitigated voltage degradation by MTO coating. In addition, the cyclability was remarkably improved and LR@MTO could maintain high capacity retention of ~81% even after 700 cycles, far surpassing the 44% of the unmodified LR and better than other oxide modified counterparts (Figure 5g, S12). Meanwhile, the reduced side reaction between cathode and electrolyte for LR@MTO served as another indicator for the inhibited oxygen loss (Figure S13). These superior electrochemical performances of LR@MTO should be attributed to the suppressed oxygen evolution after MTO surface coating.

In summary, we demonstrated that dielectric coating, in which dielectric polarization creates a reverse electric field to restrain the outward migration of bulk anions, can effectively

inhibit the oxygen evolution of Li-rich material, using Mg_2TiO_4 a model system. Detailed investigations on the underlying mechanism via DFT simulation, indicated the energy barrier of oxygen release in Li-rich material was greatly enhanced after Mg_2TiO_4 coating. Benefited from these, Mg_2TiO_4-modified Li-rich electrode showed notably reduced voltage decay with the degradation of only 151 mV after 700 cycles, compared to 432 mV of the unmodified counterpart, and exhibited significantly enhanced cyclability with a high capacity retention of ~81% at 2 C, far surpassing the 44% of the unmodified one. Our dielectric coating strategy for Li-rich cathode material not only provides an effective approach to stabilize anions of electrode materials via controlling surface chemistry, but also open a powerful avenue for unlocking the current challenges of high-energy electrode materials toward practical applications for next-generation lithium-ion batteries.

Supporting Information

Supporting Information is available from the Wiley Online Library or from the author.

Acknowledgements

This work was supported by Singapore National Research Foundation (Nanomaterials for Energy and Water Management CREATE Programme), and Energy Innovation Research Programme (EIRP) NRF2015EWT-EIRP002-008.

Received: ((will be filled in by the editorial staff))
Revised: ((will be filled in by the editorial staff))
Published online: ((will be filled in by the editorial staff))

References

[1] a) Z. Lu, D. D. MacNeil, J. R. Dahn, *Electrochem. Solid-State Lett.* **2001**, 4, A191; b) M. M. Thackeray, S.-H. Kang, C. S. Johnson, J. T. Vaughey, R. Benedek, S. Hackney, *J. Mater. Chem.* **2007**, 17, 3112; c) J. W. Choi, D. Aurbach, *Nat. Rev. Mater.* **2016**, 1, 16013; d) S. Kim, W. Cho, X. Zhang, Y. Oshima, J. W. Choi, *Nat. Commun.* **2016**, 7, 13598; e) B. Qiu, M. Zhang, L. Wu, J. Wang, Y. Xia, D. Qian, H. Liu, S. Hy, Y. Chen, K. An, *Nat. Commun.* **2016**, 7, 12108; f) J. Lee, D. A. Kitchaev, D.-H. Kwon, C.-W. Lee, J. K. Papp, Y.-S. Liu, Z. Lun, R. J. Clément, T. Shi, B. D. McCloskey, *Nature* **2018**, 556, 185; g) M. D. Radin, J. Vinckeviciute, R. Seshadri, A. Van der Ven, *Nat. Energy* **2019**, 4, 639; h) G. Assat, S. L. Glazier, C. Delacourt, J.-M. Tarascon, *Nat. Energy* **2019**, 4, 647; i) J. Hong, W. E. Gent, P. Xiao, K. Lim, D.-H. Seo, J. Wu, P. M. Csernica, C. J.

Takacs, D. Nordlund, C.-J. Sun, K. H. Stone, D. Passarello, W. Yang, D. Prendergast, G. Ceder, M. F. Toney, W. C. Chueh, *Nat. Mater.* **2019**, 18, 256; j) S. Chu, Y. Cui, N. Liu, *Nat. Mater.* **2017**, 16, 16; k) J. R. Croy, M. Balasubramanian, K. G. Gallagher, A. K. Burrell, *Acc. Chem. Res.* **2015**, 48, 2813; l) P. J. Reeves, I. D. Seymour, K. J. Griffith, C. P. Grey, *Chem. Mater.* **2019**, 31, 2814; m) S. Saha, G. Assat, M. T. Sougrati, D. Foix, H. Li, J. Vergnet, S. Turi, Y. Ha, W. Yang, J. Cabana, G. Rousse, A. M. Abakumov, J.-M. Tarascon, *Nat. Energy* **2019**, 4, 977.

[2] a) Z. Lu, J. R. Dahn, *J. Electrochem. Soc.* **2002**, 149, A815; b) M. Sathiya, G. Rousse, K. Ramesha, C. P. Laisa, H. Vezin, M. T. Sougrati, M. L. Doublet, D. Foix, D. Gonbeau, W. Walker, A. S. Prakash, M. Ben Hassine, L. Dupont, J. M. Tarascon, *Nat. Mater.* **2013**, 12, 827; c) H. Yu, H. Zhou, *J. Phys. Chem. Lett.* **2013**, 4, 1268; d) E. McCalla, A. M. Abakumov, M. Saubanère, D. Foix, E. J. Berg, G. Rousse, M.-L. Doublet, D. Gonbeau, P. Novák, G. Van Tendeloo, *Science* **2015**, 350, 1516; e) D. H. Seo, J. Lee, A. Urban, R. Malik, S. Kang, G. Ceder, *Nat. Chem.* **2016**, 8, 692; f) P. E. Pearce, A. J. Perez, G. Rousse, M. Saubanère, D. Batuk, D. Foix, E. McCalla, A. M. Abakumov, G. Van Tendeloo, M.-L. Doublet, J.-M. Tarascon, *Nat. Mater.* **2017**, 16, 580; g) M. Ben Yahia, J. Vergnet, M. Saubanere, M. L. Doublet, *Nat. Mater.* **2019**, 18, 496.

[3] a) A. R. Armstrong, M. Holzapfel, P. Novak, C. S. Johnson, S. H. Kang, M. M. Thackeray, P. G. Bruce, *J. Am. Chem. Soc.* **2006**, 128, 8694; b) M. Sathiya, A. M. Abakumov, D. Foix, G. Rousse, K. Ramesha, M. Saubanère, M. Doublet, H. Vezin, C. Laisa, A. Prakash, *Nat. Mater.* **2015**, 14, 230; c) K. Luo, M. R. Roberts, R. Hao, N. Guerrini, D. M. Pickup, Y. S. Liu, K. Edstrom, J. Guo, A. V. Chadwick, L. C. Duda, P. G. Bruce, *Nat. Chem.* **2016**, 8, 684; d) J. Zheng, S. Myeong, W. Cho, P. Yan, J. Xiao, C. Wang, J. Cho, J. G. Zhang, *Adv Energy Mater.* **2017**, 7, 1601284; e) G. Assat, J. M. Tarascon, *Nat. Energy* **2018**, 3, 373; f) H. J. Yu, Y. G. So, Y. Ren, T. H. Wu, G. C. Guo, R. J. Xiao, J. Lu, H. Li, Y. B. Yang, H. S. Zhou, R. Z. Wang, K. Amine, Y. Ikuhara, *J. Am. Chem. Soc.* **2018**, 140, 15279; g) L. de Biasi, B. Schwarz, T. Brezesinski, P. Hartmann, J. Janek, H. Ehrenberg, *Adv. Mater.* **2019**, 31, 1900985.

[4] a) J. Zheng, M. Gu, J. Xiao, B. J. Polzin, P. Yan, X. Chen, C. Wang, J.-G. Zhang, *Chem. Mater.* **2014**, 26, 6320; b) X. Zhang, I. Belharouak, L. Li, Y. Lei, J. W. Elam, A. Nie, X. Chen, R. S. Yassar, R. L. Axelbaum, *Adv Energy Mater.* **2013**, 3, 1299; c) Y. K. Sun, M. J. Lee, C. S. Yoon, J. Hassoun, K. Amine, B. Scrosati, *Adv. Mater.* **2012**, 24, 1192; d) W. Liu, P. Oh, X. Liu, S. Myeong, W. Cho, J. Cho, *Adv Energy Mater.* **2015**, 5, 1500274; e) F. Zheng, C. Yang, X. Xiong, J. Xiong, R. Hu, Y. Chen, M. Liu, *Angew. Chem. Int. Ed.* **2015**, 54, 13058; f) P. K. Nayak, J. Grinblat, M. Levi, E. Levi, S. Kim, J. W. Choi, D. Aurbach, *Adv. Energy Mater.* **2016**, 6, 1502398; g) B. Qiu, M. Zhang, L. Wu, J. Wang, Y. Xia, D. Qian, H. Liu, S. Hy, Y. Chen, K. An, Y. Zhu, Z. Liu, Y. S. Meng, *Nat. Commun.* **2016**, 7, 12108; h) J. Xie, A. D. Sendek, E. D. Cubuk, X. Zhang, Z. Lu, Y. Gong, T. Wu, F. Shi, W. Liu, E. J. Reed, Y. Cui, *ACS Nano* **2017**, 11, 7019; i) X. D. Zhang, J. L. Shi, J. Y. Liang, Y. X. Yin, J. N. Zhang, X. Q. Yu, Y. G. Guo, *Adv. Mater.* **2018**, 30, 1801751; j) Y. X. Zuo, B. A. Li, N. Jiang, W. S. Chu, H. Zhang, R. Q. Zou, D. G. Xia, *Adv. Mater.* **2018**, 30, 1707255; k) P. F. Liu, H. Zhang, W. He, T. F. Xiong, Y. Cheng, Q. S. Xie, Y. T. Ma, H. F. Zheng, L. S. Wang, Z. Z. Zhu, Y. Peng, L. Q. Mai, D. L. Peng, *J. Am. Chem. Soc.* **2019**, 141, 10876; l) S. Liu, Z. P. Liu, X. Shen, X. L. Wang, S. C. Liao, R. C. Yu, Z. X. Wang, Z. W. Hu, C. T. Chen, X. Q. Yu, X. Q. Yang, L. Q. Chen, *Adv. Energy Mater.* **2019**, 9, 1901530; m) Y. Q. Wu, H. Ming, M. L. Li, J. L. Zhang, W. Wahyudi, L. Q. Xie, X. M. He, J. Wang, Y. P. Wu, J. Ming, *ACS Energy Lett.* **2019**, 4, 656; n) T. C. Liu, A. Dai, J. Lu, Y. F. Yuan, Y. G. Xiao, L. Yu, M. Li, J. Gim, L. Ma, J. J. Liu, C. Zhan, L. X. Li, J. X. Zheng, Y. Ren, T. P. Wu, R. Shahbazian-Yassar, J. G. Wen, F. Pan, K. Amine, *Nat. Commun.* **2019**, 10, 4721; o) H.

H. Ryu, K. J. Park, D. R. Yoon, A. Aishova, C. S. Yoon, Y. K. Sun, *Adv. Energy Mater.* **2019**, 9, 1902698.

[5] a) P. Yan, J. Zheng, Z.-K. Tang, A. Devaraj, G. Chen, K. Amine, J.-G. Zhang, L.-M. Liu, C. Wang, *Nat. Nanotechnol.* **2019**, 14, 602; b) G. Assat, A. Iadecola, D. Foix, R. Dedryvere, J. M. Tarascon, *ACS Energy Lett.* **2018**, 3, 2721; c) Z. L. Chen, J. Li, X. C. Zeng, *J. Am. Chem. Soc.* **2019**, 141, 10751; d) N. Li, S. Hwang, M. Sun, Y. Fu, V. S. Battaglia, D. Su, W. Tong, *Adv. Energy Mater.* **2019**, 9, 1902258; e) Q. Li, D. Zhou, L. Zhang, D. Ning, Z. Chen, Z. Xu, R. Gao, X. Liu, D. Xie, G. Schumacher, X. Liu, *Adv. Funct. Mater.* **2019**, 29, 1806706; f) E. Hu, X. Yu, R. Lin, X. Bi, J. Lu, S. Bak, K.-W. Nam, H. L. Xin, C. Jaye, D. A. Fischer, *Nat. Energy* **2018**, 3, 690; g) S. Sharifi-Asl, J. Lu, K. Amine, R. Shahbazian-Yassar, *Adv Energy Mater.* **2019**, 9, 1900551.

[6] a) F. Lin, I. M. Markus, D. Nordlund, T. C. Weng, M. D. Asta, H. L. Xin, M. M. Doeff, *Nat. Commun.* **2014**, 5, 3529; b) R. Benedek, H. Iddir, *J. Phys. Chem. C* **2017**, 121, 6492; c) B. Strehle, K. Kleiner, R. Jung, F. Chesneau, M. Mendez, H. A. Gasteiger, M. Piana, *J. Electrochem. Soc.* **2017**, 164, A400; d) X. Li, Y. Qiao, S. Guo, Z. Xu, H. Zhu, X. Zhang, Y. Yuan, P. He, M. Ishida, H. Zhou, *Adv. Mater.* **2018**, 30, 1705197.

[7] a) B. Li, N. Jiang, W. Huang, H. Yan, Y. Zuo, D. Xia, *Adv. Funct. Mater.* **2018**, 28, 1704864; b) L. F. Zou, W. G. Zhao, Z. Y. Liu, H. P. Jia, J. M. Zheng, G. F. Wang, Y. Yang, J. G. Zhang, C. M. Wang, *ACS Energy Lett.* **2018**, 3, 2433; c) W. Zhang, L. Cai, S. Cao, L. Qiao, Y. Zeng, Z. Zhu, Z. Lv, H. Xia, L. Zhong, H. Zhang, X. Ge, J. Wei, S. Xi, Y. Du, S. Li, X. Chen, *Adv. Mater.* **2019**, 31, 1906156.

[8] a) D. Qian, B. Xu, M. Chi, Y. S. Meng, *Phys. Chem. Chem. Phys.* **2014**, 16, 14665; b) D. Wang, T. Xu, Y. Li, D. Pan, X. Lu, Y.-S. Hu, S. Dai, Y. Bai, *ACS Appl. Mater. Interfaces* **2018**, 10, 41802; c) S. Li, S.-J. Lee, X. Wang, W. Yang, H. Huang, D. S. Swetz, W. B. Doriese, G. C. O'Neil, J. N. Ullom, C. J. Titus, K. D. Irwin, H.-K. Lee, D. Nordlund, P. Pianetta, C. Yu, J. Qiu, X. Yu, X.-Q. Yang, E. Hu, J.-S. Lee, Y. Liu, *J. Am. Chem. Soc.* **2019**, 141, 12079.

[9] a) S. F. Li, S. J. Lee, X. L. Wang, W. L. Yang, H. Huang, D. S. Swetz, W. B. Doriese, G. C. O'Neil, J. N. Ullom, C. J. Titus, K. D. Irwin, H. K. Lee, D. Nordlund, P. Pianetta, C. Yu, J. S. Qiu, X. Q. Yu, X. Q. Yang, E. Y. Hu, J. S. Lee, Y. J. Liu, *J. Am. Chem. Soc.* **2019**, 141, 12079; b) W. D. Li, H. Y. Asl, Q. Xie, A. Manthiram, *J. Am. Chem. Soc.* **2019**, 141, 5097; c) Z. N. Taylor, A. J. Perez, J. A. Coca-Clemente, F. Braga, N. E. Drewett, M. J. Pitcher, W. J. Thomas, M. S. Dyer, C. Collins, M. Zanella, T. Johnson, S. Day, C. Tang, V. R. Dhanak, J. B. Claridge, L. J. Hardwick, M. J. Rosseinsky, *J. Am. Chem. Soc.* **2019**, 141, 7333; d) X. Li, Y. Qiao, S. H. Guo, K. Z. Jiang, M. Ishida, H. S. Zhou, *Adv. Mater.* **2019**, 31, 1807825.

[10] a) T. Teufl, B. Strehle, P. Müller, H. A. Gasteiger, M. A. Mendez, *J. Electrochem. Soc.* **2018**, 165, A2718; b) J. C. Zhang, F. Y. Cheng, S. L. Chou, J. L. Wang, L. Gu, H. Wang, H. Yoshikawa, Y. Lu, J. Chen, *Adv. Mater.* **2019**, 31, 1901808.

[11] a) B. Song, W. Li, S.-M. Oh, A. Manthiram, *ACS Appl. Mater. Interfaces* **2017**, 9, 9718; b) C. Yada, A. Ohmori, K. Ide, H. Yamasaki, T. Kato, T. Saito, F. Sagane, Y. Iriyama, *Adv. Energy Mater.* **2014**, 4, 1301416.

[12] a) S. J. Hu, Y. Li, Y. H. Chen, J. M. Peng, T. F. Zhou, W. K. Pang, C. Didier, V. K. Peterson, H. Q. Wang, Q. Y. Li, Z. P. Guo, *Adv. Energy Mater.* **2019**, 9, 1901795; b) T. Deng, X. L. Fang, L. S. Cao, J. Chen, S. Y. Hou, X. Ji, L. Chen, S. Li, X. Q. Zhou, E. Y. Hu, D. Su, X. Q. Yang, C. S. Wang, *Joule* **2019**, 3, 2550; c) Y. Pei, Q. Chen, Y.-C. Xiao, L. Liu, C.-Y. Xu, L. Zhen, G. Henkelman, G. Cao, *Nano energy* **2017**, 40, 566; d) A. Singer, M. Zhang, S. Hy, D. Cela, C. Fang, T. A. Wynn, B. Qiu, Y. Xia, Z. Liu, A. Ulvestad, N. Hua, J. Wingert, H. Liu, M. Sprung, A. V. Zozulya, E. Maxey, R. Harder, Y. S. Meng, O. G. Shpyrko, *Nat. Energy* **2018**, 3, 641; e) J. L. Shi, D. D. Xiao, M. Y.

Ge, X. Q. Yu, Y. Chu, X. J. Huang, X. D. Zhang, Y. X. Yin, X. Q. Yang, Y. G. Guo, L. Gu, L. J. Wan, *Adv. Mater.* **2018**, 30, 1705575.

[13] D. Luo, G. Li, C. Fu, J. Zheng, J. Fan, Q. Li, L. Li, *Adv Energy Mater*. **2014**, 4, 1400062.

[14] a) R. C. Weast, M. J. Astle, W. H. Beyer, *CRC handbook of chemistry and physics*, Vol. 69, CRC press Boca Raton, FL, **1988**; b) N. J. Stalter, Google Patents, **1972**; c) P. K. Nayak, J. Grinblat, E. Levi, M. Levi, B. Markovsky, D. Aurbach, *Phys. Chem. Chem. Phys.* **2017**, 19, 6142; d) D. Kong, J. Hu, Z. Chen, K. Song, C. Li, M. Weng, M. Li, R. Wang, T. Liu, J. Liu, M. Zhang, Y. Xiao, F. Pan, *Adv. Energy Mater.* **2019**, 9, 1901756; e) F. L. Wu, G. T. Kim, M. Kuenzel, H. Zhang, J. Asenbauer, D. Geiger, U. Kaiser, S. Passerini, *Adv. Energy Mater.* **2019**, 9, 1902445.

[15] a) M. J. Martínez-Lope, M. P. Baura-Peña, M. E. Garíca-Clavel, *Thermochim. Acta* **1992**, 194, 59; b) H. Cui, H. Li, J. Liu, Y. Zhang, F. Cheng, J. Chen, *Inorg. Chem. Front.* **2019**, 6, 1694; c) Y. Zhang, Y. Tang, J. Deng, W. R. Leow, H. Xia, Z. Zhu, Z. Lv, J. Wei, W. Li, C. Persson, O. I. Malyi, M. Antonietti, X. Chen, *ACS Mater. Lett.* **2019**, 1, 519; d) W. Zhang, X. Sun, Y. Tang, H. Xia, Y. Zeng, L. Qiao, Z. Zhu, Z. Lv, Y. Zhang, X. Ge, S. Xi, Z. Wang, Y. Du, X. Chen, *J. Am. Chem. Soc.* **2019**, 141, 14038.

[16] a) O. Schilling, J. Dahn, *J. Electrochem. Soc.* **1998**, 145, 569; b) H. B. Kim, B. C. Park, S. T. Myung, K. Amine, J. Prakash, Y. K. Sun, *J. Power Sources* **2008**, 179, 347; c) K.-W. Nam, S.-M. Bak, E. Hu, X. Yu, Y. Zhou, X. Wang, L. Wu, Y. Zhu, K.-Y. Chung, X.-Q. Yang, *Adv. Funct. Mater.* **2013**, 23, 1047.

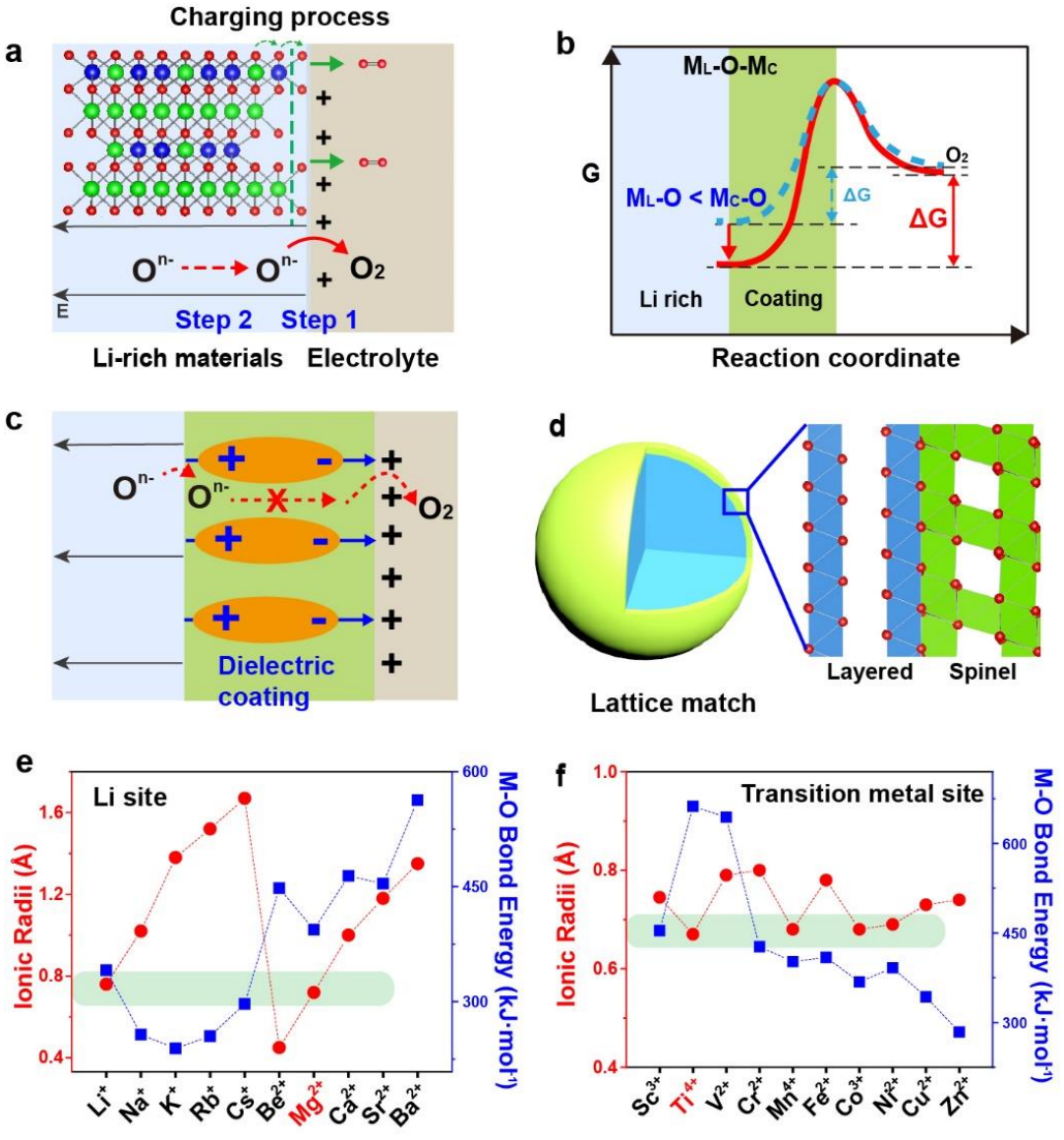

Scheme 1. (a) Schematic illustration of the continuous oxygen release process of Li-rich cathode materials during charging. Step 1. Surface oxygen loss. Step 2. Outward migration of bulk oxygen. (b) The proposed surface modification with elements exhibiting high oxygen-affinity to make the surface oxygen evolution reaction energetically unfavorable. M_L-O and M_C-O represent the chemical bond between metal and oxygen in Li-rich and coating materials, respectively. (c) The proposed dielectric coating to inhibit the outward migration of oxygen anions. (d) Spinel coating owns almost the same oxygen arrangement with layered Li-rich materials, ensuring structural compatibility. (e-f) Element selection for dielectric coating in (e) Li and (f) transition-metal sites based on two criteria, ionic radii and M-O bond energy.

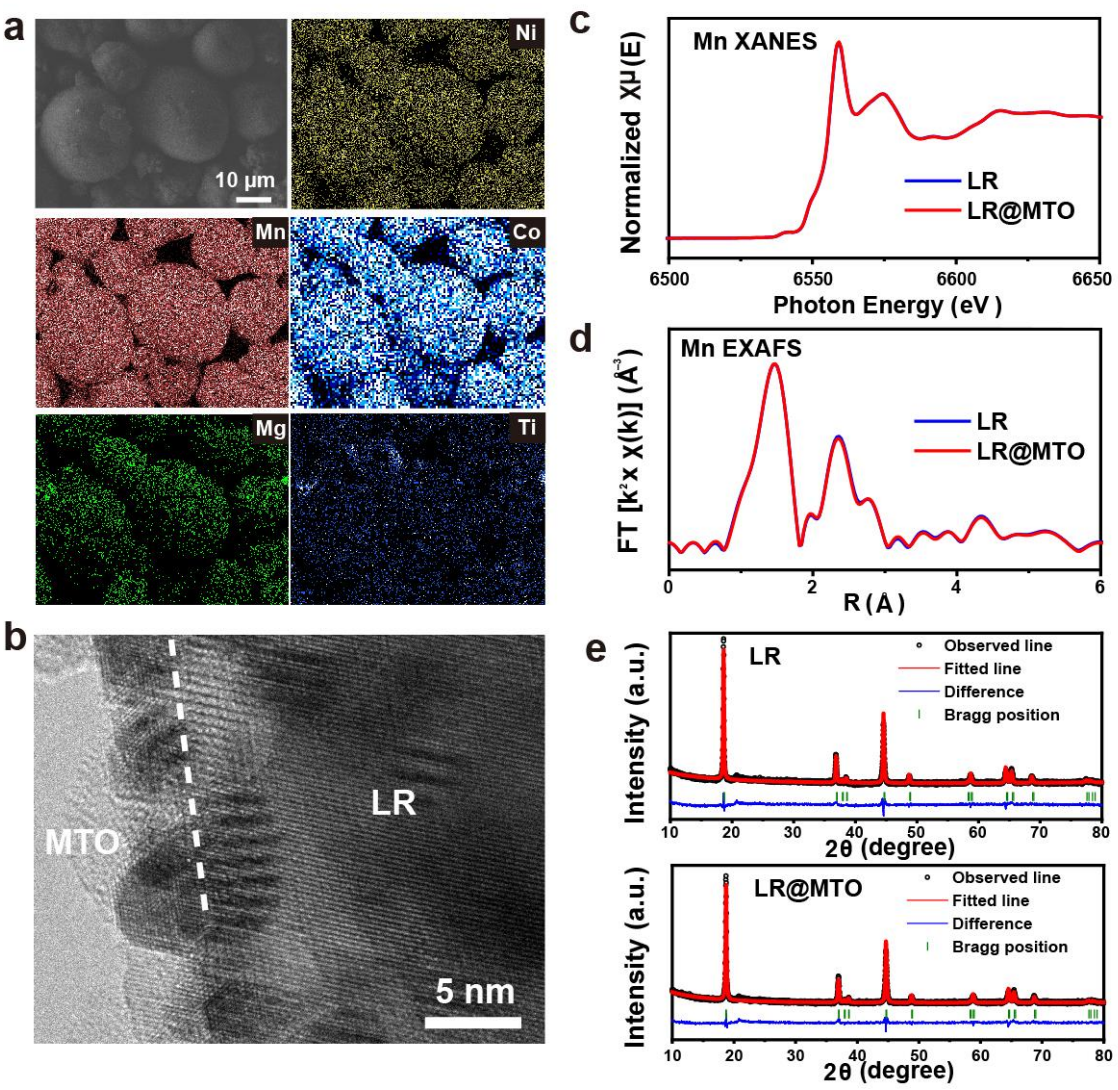

Figure 1. a) SEM image and elemental mapping of Ni, Mn, Co, Mg, and Ti for LR@MTO. b) HRTEM image of LR@MTO. c) Mn XANES and d) Mn EXAFS of LR and LR@MTO. e) XRD patterns and the corresponding Rietveld refinement of LR and LR@MTO. LR@MTO exhibits almost the same XAS and XRD results with LR, indicating the coating process doesn't change the bulk structure of LR.

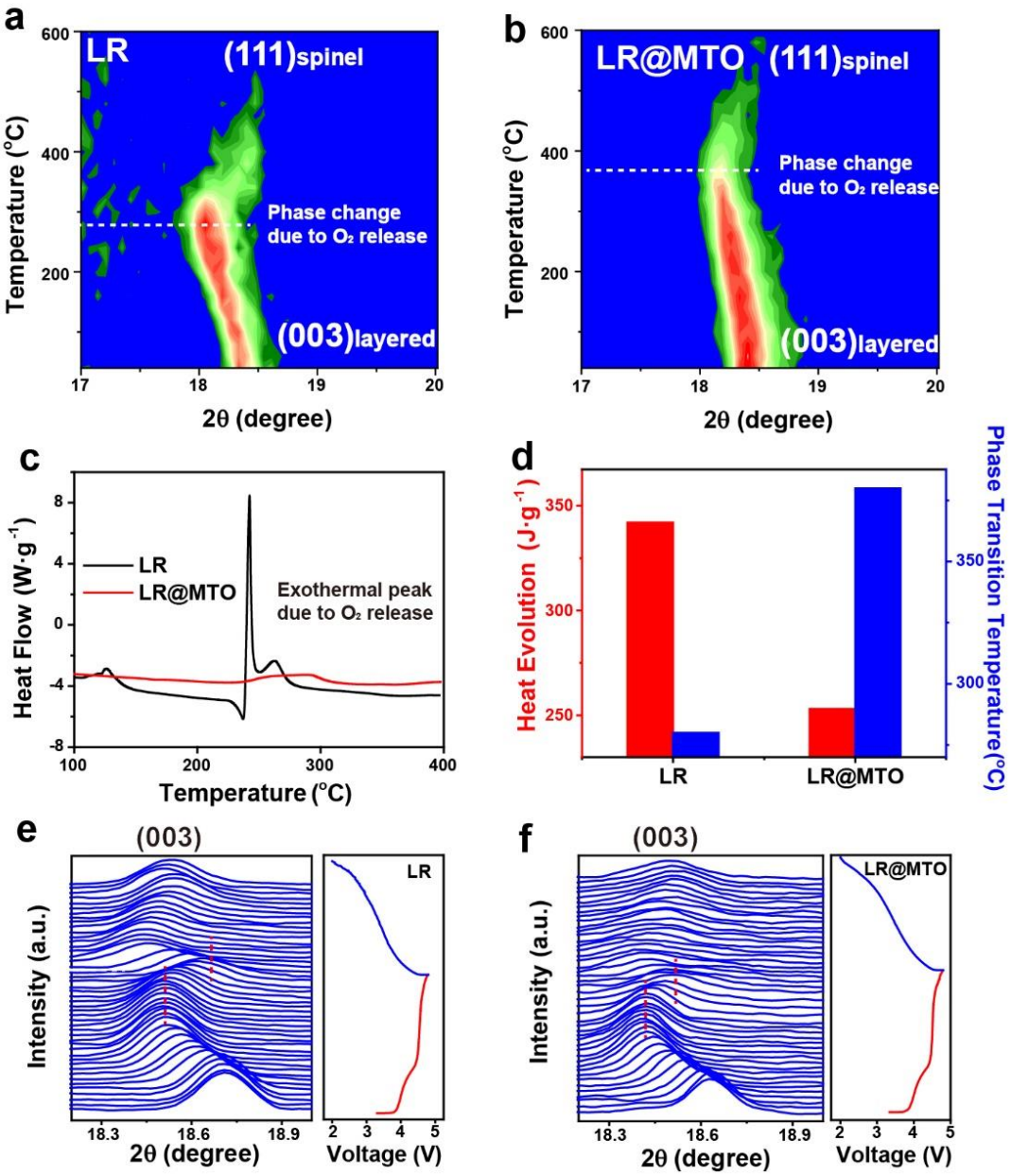

Figure 2. a, b) In situ XRD results of fully-charged a) LR and b) LR@MTO electrodes during heating experiment, showing that bare LR goes through phase transformation at lower temperature than the LR@MTO. c) DSC study of the thermal stability for fully-charged LR and LR@MTO electrodes. d) Comparison of heat evolution and phase transition temperature between LR and LR@MTO. e, f) In situ XRD patterns of e) LR and f) LR@MTO during the charging/discharging process at the first cycle. The higher angle (003) reflection shifts, the more severe oxygen release. These results indicate the suppressed oxygen loss after MTO coating.

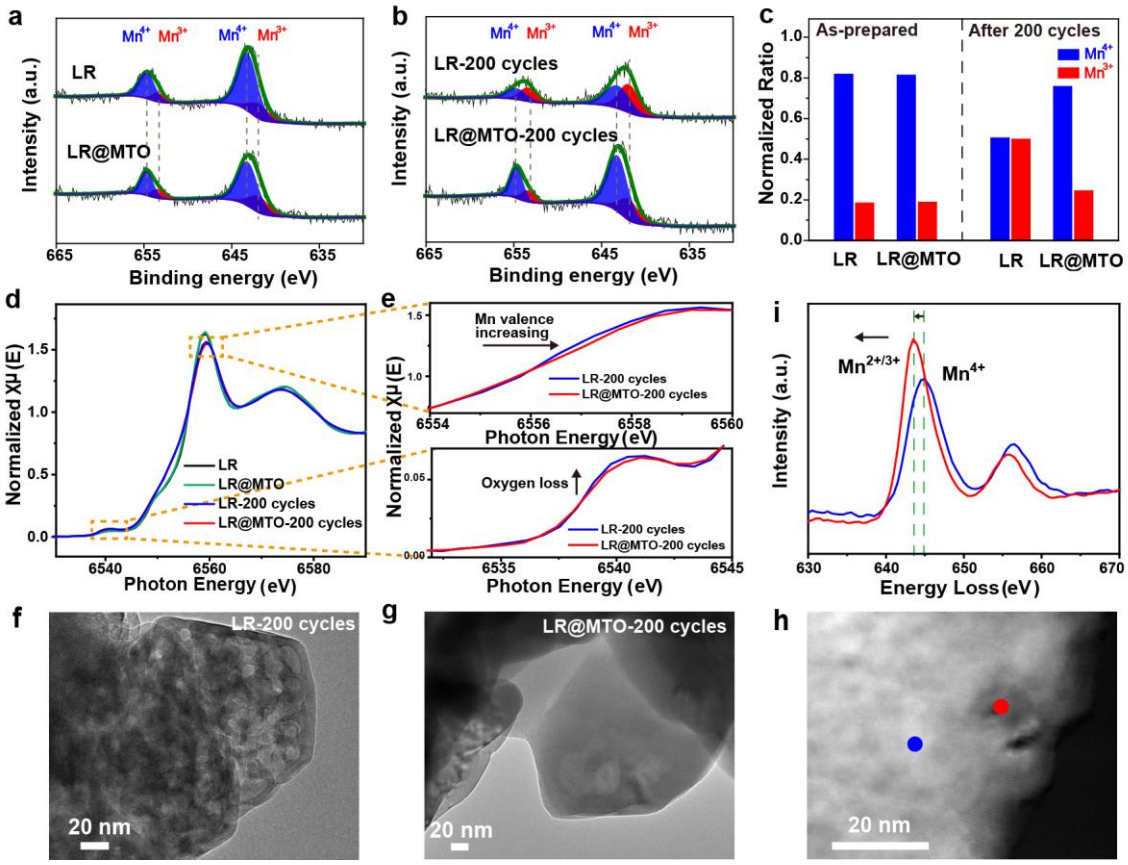

Figure 3. a, b) Mn 2p XPS spectra of a) as-prepared and b) post-cycled LR and LR@MTO at 2 C. c) Normalized Mn^{3+}/Mn^{4+} ratio based on XPS results. d) Mn-edge XANES of LR, LR@MTO and these after 200 cycles. e) Enlarged view of XANES for LR and LR@MTO after 200 cycles marked with the small square in d). f, g) TEM images of post-cycled f) LR and g) LR@MTO. h) STEM image of LR after 200 cycles and i) Mn EELS profiles detected at the two points marked in h).

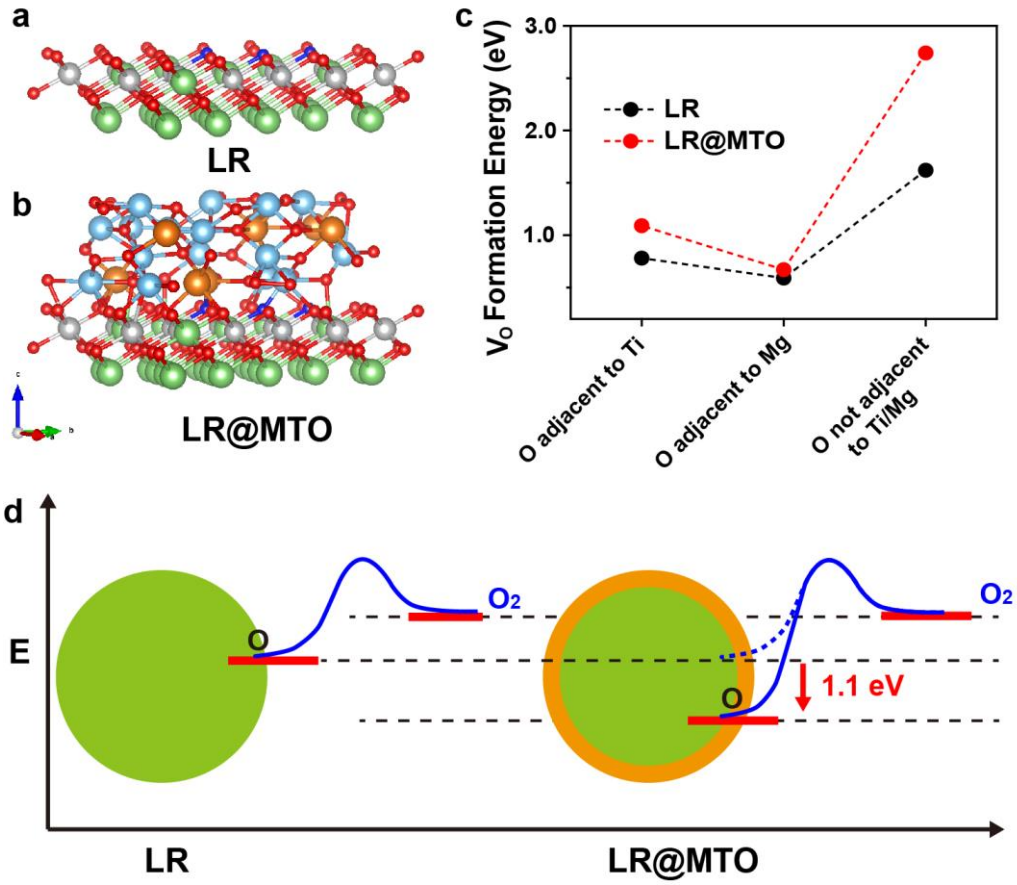

Figure 4. a, b) Crystal structures of relaxed bare a) and MTO-modified b) LR (003) surfaces. Red spheres represent oxygen, silver spheres are manganese, nickel, and cobalt, green spheres represent lithium, brown spheres are magnesium, and blue spheres are titanium. V_o means oxygen vacancy. c) Formation energy of oxygen vacancies on the surface of LR and LR@MTO. d) Schematic illustration of the impact of MTO coating on the formation energy of surface oxygen vacancies in LR cathode material.

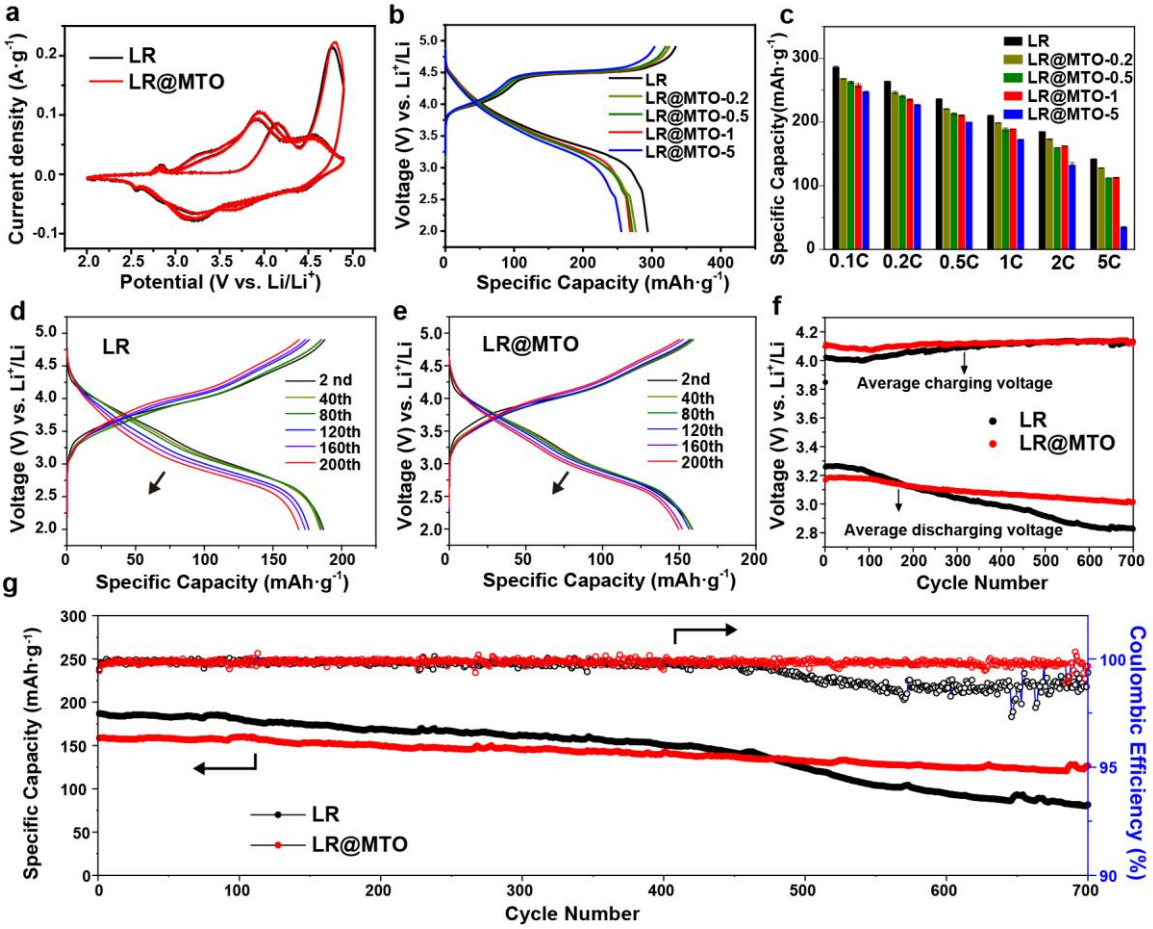

Figure 5. a) Cyclic voltammetry of the first three cycles for LR and LR@MTO at a sweep rate of 0.1 $mV \cdot s^{-1}$ within the potential range from 2 to 4.9 V vs Li^+/Li. b) Charging-discharging curves at 0.1 C and c) rate performance of LR and LR@MTO with varied amounts of coating. d, e) Charging discharging curves of LR and LR@MTO of different cycles ranging from 2^{nd}, 40^{th}, 80^{th}, 120^{th}, 160^{th}, and 200^{th} at 2 C. f) Average discharging and charging voltage of LR and LR@MTO with cycling. g) Cycle performances of LR and LR@MTO at 2 C.

Dielectric inverse spinel structured Mg_2TiO_4 coating on Li-rich cathode material significantly suppresses the continuous oxygen release, endowing batteries with remarkable cyclability and well-inhibited voltage decay, e.g., showing a capacity retention of ~81% and voltage degradation of only 151 mV after 700 cycles, far superior to 44% and 432 mV of the unmodified counterpart.

Keyword: dielectric polarization, cathode materials, oxygen release, surface modification, lithium-ion batteries

Wei Zhang, Yonggang Sun, Huiqiu Deng, Jianming Ma, Yi Zeng, Zhiqiang Zhu, Zhisheng Lv, Huarong Xia, Xiang Ge, Shengkai Cao, Yao Xiao, Shibo Xi, Yonghua Du, Anmin Cao and Xiaodong Chen**

Dielectric Polarization in Inverse Spinel-Structured Mg_2TiO_4 Coating to Suppress Oxygen Evolution of Li-Rich Cathode Materials

TOC figure